Am J Physiol Heart Circ Physiol 291: H2617–H2629, 2006.
First published July 7, 2006; doi:10.1152/ajpheart.00350.2006.

CALL FOR PAPERS | *Computational Analyses in Ion Channelopathies*

Contributions of sustained I_{Na} and I_{Kv43} to transmural heterogeneity of early repolarization and arrhythmogenesis in canine left ventricular myocytes

Sarah N. Flaim, Wayne R. Giles, and Andrew D. McCulloch
Department of Bioengineering, University of California, San Diego, La Jolla, California

Submitted 31 March 2006; accepted in final form 29 June 2006

Flaim, Sarah N., Wayne R. Giles, and Andrew D. McCulloch. Contributions of sustained I_{Na} and I_{Kv43} to transmural heterogeneity of early repolarization and arrhythmogenesis in canine left ventricular myocytes. *Am J Physiol Heart Circ Physiol* 291: H2617–H2629, 2006. First published July 7, 2006; doi:10.1152/ajpheart.00350.2006.—The roles of sustained components of I_{Na} and I_{Kv43} in shaping the action potentials (AP) of myocytes isolated from the canine left ventricle (LV) have not been studied in detail. Here we investigate the hypothesis that these two currents can contribute substantially to heterogeneity of early repolarization and arrhythmic risk. Quantitative data from voltage-clamp and expression profiling experiments were used to complete meaningful modifications to an existing "local control" model of canine midmyocardial myocyte excitation-contraction coupling for epicardial and endocardial cells. We include *1*) heterogeneous I_{Kv43}, I_{Ks}, and I_{SERCA} density; *2*) modulation of I_{Kv43} by Kv channel interacting protein type 2 (KChIP2) channel subunits; *3*) a possible Ca^{2+}-dependent open-state inactivation of I_{Kv43}; and *4*) a sustained component of the inward Na^+ current, I_{NaL}. The resulting simulations illustrate ways in which KChIP2- and Ca^{2+}-dependent control of I_{Kv43} can result in a sustained outward current that can neutralize I_{NaL} in a rate- and myocyte subtype-dependent manner. Both these currents appear to play significant roles in modulating AP duration and rate dependence in midmyocardial myocytes. Furthermore, an increased ratio of I_{Kv43} to I_{NaL} is capable of protecting epicardial myocytes from the early afterdepolarizations resulting from the SCN5A-I1768V mutation-induced increase in I_{NaL}. Experimentally observed transmural differences in Ca^{2+} handling, including greater sarcoplasmic reticulum Ca^{2+} content and faster Ca^{2+} transient decay rates on the epicardium, were recapitulated in our simulations. By design, these models allow upward integration into organ models or may be used as a basis for further investigations into cellular heterogeneities.

sustained sodium ion current; Kv4 channel regulation

SIGNIFICANT DIFFERENCES in the expression patterns of a number of ion channels are an important functional distinction among cells isolated from the left ventricular (LV) endocardium, epicardium, and midmyocardium of many species, including human (12, 27), dog (3, 54), guinea pig (3), rabbit (33), and mouse (6). The major consequence of this systematic variation in ionic currents is a corresponding heterogeneity of action potential duration (APD), waveform, and rate dependence (27). It is hypothesized that these so-called intrinsic electrophysiological differences are responsible for a normal sequence of activation and repolarization in healthy hearts. Moreover, either exaggeration or significant reductions of repolarization heterogeneities, due to drug actions, inherited mutations, or acquired disease, may be proarrhythmic. Experimental studies in ventricular myocytes have begun to define the molecular and ionic mechanisms underlying the transmural heterogeneities of ion channel and calcium (Ca^{2+})-handling proteins. A relatively extensive data set is now available for the canine ventricular myocardium. The ionic currents that are known to exhibit transmural heterogeneities include the transient outward potassium (K^+) current, I_{Kv43}(30); the slowly activating delayed rectifier K^+ current, I_{Ks} (29); the late sodium (Na^+) current, I_{NaL} (68); the Na^+/Ca^{2+} exchanger, I_{NaCa} (62, 69); and the sarcoplasmic reticulum (SR) Ca^{2+}-ATPase uptake rate, I_{SERCA} (25). Important unresolved questions concerning the functional importance of these transmural heterogeneities remain.

This study was motivated by the possibility that we could integrate data concerning *1*) known heterogeneities, to determine whether they are sufficient to explain the distinct AP waveforms; and *2*) information regarding known interactions between the subunits comprising an ion channel, to reproduce channel function within intact myocytes and explore the functional roles of these interactions. Computational modeling provides a useful framework with which to integrate extensive experimental data and develop specific working hypotheses to guide quantitative investigations into these unresolved questions.

The ionic mechanisms responsible for the intrinsically long APDs and pronounced rate dependence of midmyocardial myocytes in the LV have been the focus of many experimental investigations (2). Most previous hypotheses have been centered on the relatively large K^+ outward currents that are responsible for late repolarization (phase 3). However, evidence is emerging that some currents previously measured and defined as being transient (such as both I_{Na} and I_{Kv43}) modulate APD as a consequence of their smaller slowly inactivating or sustained components. The relatively high resistance of the ventricular AP plateau provides a substrate in which these small net currents can modulate the AP waveform (56). In this study, we have investigated the hypothesis that these two currents can contribute substantially to early repolarization. As such, transmural differences in these currents may lead to increased APD and arrhythmogenic risk of midmyocardial myocytes.

Address for reprint requests and other correspondence: A. McCulloch, Univ. of California, San Diego, Dept. of Bioengineering, 9500 Gilman Drive MC 0412, La Jolla, CA 92093-0412 (e-mail: amcculloch@ucsd.edu).

The costs of publication of this article were defrayed in part by the payment of page charges. The article must therefore be hereby marked "*advertisement*" in accordance with 18 U.S.C. Section 1734 solely to indicate this fact.

Intracellular Ca^{2+} cycling is an important regulator of normal and abnormal excitation-contraction coupling (ECC) (4). In the myoplasm, Ca^{2+} binds to regulatory molecules, such as calmodulin, and thereby can modify ion channel function on a beat-to-beat basis or over longer time periods (43). Furthermore, Ca^{2+}-mediated early afterdepolarizations (EADs) can facilitate the development of potentially life-threatening reentrant arrhythmias by increasing transmural dispersion of repolarization. In an effort to create a mechanistic yet computationally efficient model of Ca^{2+} cycling in the cardiac ventricular myocyte, Hinch et al. (19) used a method based on time scale decomposition to simplify continuous-time Markov chain descriptions of L-type Ca^{2+} channel (LCC) and ryanodine receptor (RyR) gating. This resulted in a low-order system of ordinary differential equations (ODEs) representing the ensemble behavior of the so-called Ca^{2+} release units (comprising 1 LCC and 5 RyRs) while also retaining many key biophysical properties (19). Greenstein et al. (15) generalized this approach to allow LCC and RyR models of arbitrary complexity and combined this model with their equations for ionic currents in canine midmyocardial myocytes. The resulting whole-cell model was shown to faithfully reproduce features of LCC voltage and Ca^{2+} sensitivity, ECC, and AP and Ca^{2+} cycling properties of a canine midmyocardial myocyte (15).

The time- and voltage-dependent properties of the Kv4.3 channel current are now known to be much more complex than previous models accounted for. This is, at least in part, due to accessory β-subunits, such as the K^+ channel interacting proteins (KChIPs). Specifically, KChIP isoforms both promote cell surface expression and modify gating kinetics (42). Furthermore, it has been suggested that the steep transmural gradient of KChIP expression may contribute to the heterogeneous measurements of I_{Kv43} across the canine LV wall (48, 66). Patel et al. (42) propose that once Kv4.3 channels transition to the open state, inactivation can occur via two distinct mechanistic pathways: a Ca^{2+}-independent closed-state mechanism or a Ca^{2+}-dependent open-state mechanism. However, at present it is unknown whether these results, obtained in heterologous systems, are relevant to the cardiac myocyte AP waveform or ECC.

In this study, we completed meaningful modifications to the Greenstein model (15) of canine midmyocardial myocyte ECC for epicardial and endocardial cells. We accomplished this by utilizing recent experimental data describing the molecular basis of transmural cellular heterogeneity and existing Markov models of I_{NaL} and I_{Kv43}. We first demonstrate the ability of the models to simulate quantitative features of regionally varying ion channel function or expression levels. Next, we explore the consequences of a possible Ca^{2+}-dependent inactivation of I_{Kv43} on the canine LV AP waveforms. Finally, we investigate the contributions of sustained components of I_{NaL} and I_{Kv43} to early repolarization and transmural heterogeneities of APD in canine LV myocytes. We also explore how an increase in I_{NaL}, e.g., due to the SCN5A-I1768V mutation, may contribute to regional increases in APD and arrhythmic risk, examine potential additional heterogeneities, and suggest targets for further experimental investigation. This particular mutation was selected because it modifies the sustained component of I_{Na} and, as such, may differentially alter AP values measured in myocytes isolated from different regions across the LV wall. These models are biophysically detailed, yet computationally tractable, allowing for upward integration into tissue- and organ-scale models.

METHODS

The Greenstein model of ECC in a canine midmyocardial myocyte (15) was used as a basis for the three canine ventricular myocyte models in this study. Briefly, the original model consists of 76 ODEs, of which 40 represent intracellular Ca^{2+} cycling states. The other 36 ODEs represent gating kinetics and ion transfer relationships of the known ion channels and corresponding Na^+, Ca^{2+}, K^+, and Cl^- currents. We added an extra state variable representing open-state inactivation of I_{Kv43} (42) and replaced the existing Hodgkin-Huxley equations (3 state variables) with a 13-state Markov model of I_{Na} (7). Thus our modified models comprised 87 ODEs. The ionic currents we have included as contributors to transmurally heterogeneous AP values are outlined below. A summary of the original and modified parameters is provided in Table S1 of the Supplemental Data.[1] Experimental data used for model validation were converted to a digital format and digitized using MATLAB.

The transient outward K^+ current, I_{Kv43}. This K^+ conductance is an important regulator of the early repolarization phase of the AP. Furthermore, changes in I_{Kv43} can modify ECC in ventricular myocytes (51). To investigate the consequences of a Ca^{2+}-dependent open-state inactivation of I_{Kv43}, as proposed by Patel et al. (42), we incorporated an additional state into the existing homotetrameric Markov model of Greenstein et al. (17) (see Fig. S1 in the Supplemental Data). Specifically, the scaling factor for Kv4.3 (controlling current amplitude), the recovery from inactivation transition rate α_i, and the closed-state inactivation transition rate β_i were modified so that they agreed with recent experimental data (Supplemental Table S1). The Ca^{2+}-dependent inactivation from the open state was simulated by the inclusion of an additional state variable I_o, and two transition rates, $\alpha_{o,i}$ and $\beta_{o,i}$. Since KChiP2 modifies only the Kv4.3 current (not Kv1.4 current), we altered only the biophysical parameters corresponding to Kv4.3. In the absence of any data to the contrary, we assumed that Kv1.4 is homogeneously expressed across the wall of the adult canine LV.

Voltage-clamp data from Rosati et al. (48) suggests that the current density of the transient outward current (I_{to1}) from the epicardium of the canine LV is 36% larger and that I_{to1} from the endocardium is 80% smaller than in the midmyocardium. We used these data to estimate Kv4.3 scaling factors for epicardial and endocardial myocytes relative to the original value in the midmyocardial model (15). All three values were adjusted to closely match the voltage-clamp data of Liu et al. (30) (although they found no statistical significant difference between epicardial and midmyocardial I_{Kv43}). The KChIP2-dependent transition rates (α_i, β_i) were altered to match data from Patel et al. (42). Their data and this adjustment are based on an abundance of KChIP2 subunits on the epicardium and virtually no KChIP2 subunits on the endocardium. The corresponding midmyocardial transition rates were estimated by interpolating between epicardial and endocardial values using the measured gradient of KChIP2 mRNA expression of Rosati et al. (48). Since the kinetic measurements of I_{Kv43} were performed at 22°C, all transition rates were scaled up to account for temperature dependence of this current.

The fourth EF-hand moiety of the KChIP β-subunit displays the highest Ca^{2+} affinity and underlies most of the Ca^{2+} sensitivity. We have assumed that the Ca^{2+}-dependent transition rate $\alpha_{o,i}$ is linearly dependent on cytosolic Ca^{2+} concentration ($[Ca^{2+}]_i$). The formulation of the transition rate controlling recovery from open-state inactivation ($\beta_{o,i}$) was based on the voltage-dependent deactivation transition rate, β_a, but scaled to result in an appropriate rate of current inactivation. The relative contribution of the K^+ channel α-subunit

[1] The online version of this article contains supplemental data.

transcripts Kv4.3 to Kv1.4 was adjusted slightly from 77%/23% to 85%/15% to match the data of Dixon et al. (11). After all transition rate modifications were made, Kv4.3 scaling factors were readjusted to yield appropriate peak currents.

The slowly inactivating or late Na^+ current, I_{NaL}. To account for this important biophysical property of I_{Na}, we replaced the existing Hodgkin-Huxley formulation with the Markov model of Clancy et al. (7). This version includes both a background mode, contributing predominantly to the large transient component of I_{Na}, and a burst mode, which is activated during the plateau phase of the AP and results in a sustained inward current of roughly 0.07% of the peak current density. The background mode also contributes to a second, albeit much smaller (0.2%), current density peak during phase 3 repolarization or a ramped voltage-clamp protocol (7). The magnitude of the channel conductance was reduced to 4.6 mS/μF to yield a similar peak current density (~300 pA/pF) in both the Hodgkin-Huxley and Markov formulations.

Experimental evidence suggests that not all SCN5A channels exhibit this bursting behavior. Furthermore, the data of Zygmunt et al. (68) indicate that I_{NaL} is approximately twice as great in the midmyocardium as in the other regions. To reflect this heterogeneity, we reduced the bursting state conductance to one-fourth of the background conductance in endocardial and epicardial myocytes and one-half of the background conductance in midmyocardial myocytes. To model the I1768V mutation, we increased the recovery kinetics as described by Clancy et al. (7), although to a lesser extent (50% increase instead of 100%). This resulted in an equivalent increase in I_{NaL} in response in a ramped voltage protocol.

The slowly activating delayed rectifier current, I_{Ks}. Our I_{Ks} current formulation is the same as that of Winslow et al. (60). However, we modified the maximal conductance in the three types of canine ventricular myocyte in order to yield tail current densities that match the experimental values of Liu and Antzelevitch (29). Specifically, the statistically significant difference in midmyocardial tail currents was accounted for in our model.

Transmural variation in Ca^{2+}-handling proteins. To model heterogeneity of the SERCA uptake rate, we included a scaling term for both the forward and reverse rate of the existing SERCA pump model, as has been done by Iyer et al. (21). SR uptake in epicardial myocytes was increased by a factor of 2.0, as suggested by the data of Laurita et al. (25).

Computational methods and analysis. All simulations were implemented and executed in MATLAB using the built-in ode23t integrator with a maximum step size of 0.1 ms. APD was computed at 30% and 90% repolarization (APD_{30} and APD_{90}). We fitted exponential functions to the inactivation and recovery curves of I_{Kv43} in a manner similar to Patel et al. (42). Briefly, for $\tau_{closed,inact}$ and τ_f, the time constants were obtained by fitting exponentials of the form $I = A_1\exp(-t/\tau)$. For τ_{rec}, the time constants were obtained by fitting exponentials of the form $I = I_{peak}[1 - \exp(-t/\tau_{rec})]$.

RESULTS

The transient outward K^+ current, I_{Kv43}. Families of simulated current tracings corresponding to I_{Kv43} in epicardial, midmyocardial, and endocardial myocytes are shown in Fig. 1*A*. The voltage clamp protocol is illustrated in the *inset*. The peak currents are plotted in Fig. 1*B* along with experimental results of Liu et al. (30) for comparison. These predicted I_{Kv43} amplitudes for each canine ventricular myocyte subtype are also consistent with published current amplitudes in a number of previous papers (35, 48, 66). Note that Liu et al. (30) did not detect significant differences between epicardial and midmyocardial myocytes. We chose to use the more complete data of Rosati et al. (48) as a basis for the I_{Kv43} scaling parameters. Hence, our model predicts a slightly larger difference in peak I_{Kv43} between epicardial and midmyocardial cells, although this is still within the range of experimental variation.

The simulations in Fig. 2 demonstrate the ability of our model to account for differences in the gating kinetics of Kv4.3 that have been reported in the presence and absence of KChIP2 accessory subunits. Since the experimental results for different KChIP2 isoforms (KChIP2b and KChIP2d) were in general very similar, these data have been averaged. In our simulations,

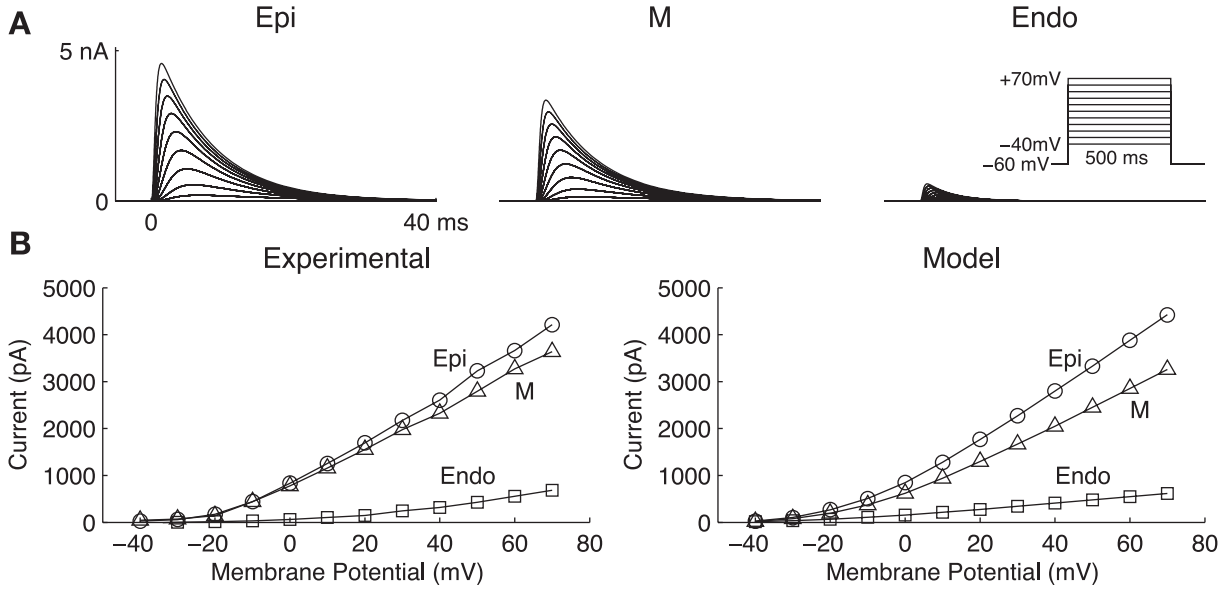

Fig. 1. Heterogeneity of I_{Kv43} in epicardial (Epi), midmyocardial (M), and endocardial (Endo) canine left ventricular (LV) myocytes. *A*: predicted I_{Kv43} current tracings in all three ventricular myocytes subtypes at 37°C (including voltage-clamp protocol). The tracings were recorded during depolarizing steps (300-ms duration) from a holding potential of −80 mV to test potentials ranging from −40 to +70 mV. The time scale of the record is abbreviated in order to better illustrate differences in these currents. *B*: peak current measurements from the voltage-clamp protocol in *A* measured by Liu et al. (30) at 37°C (*left*) and predicted by the model (*right*).

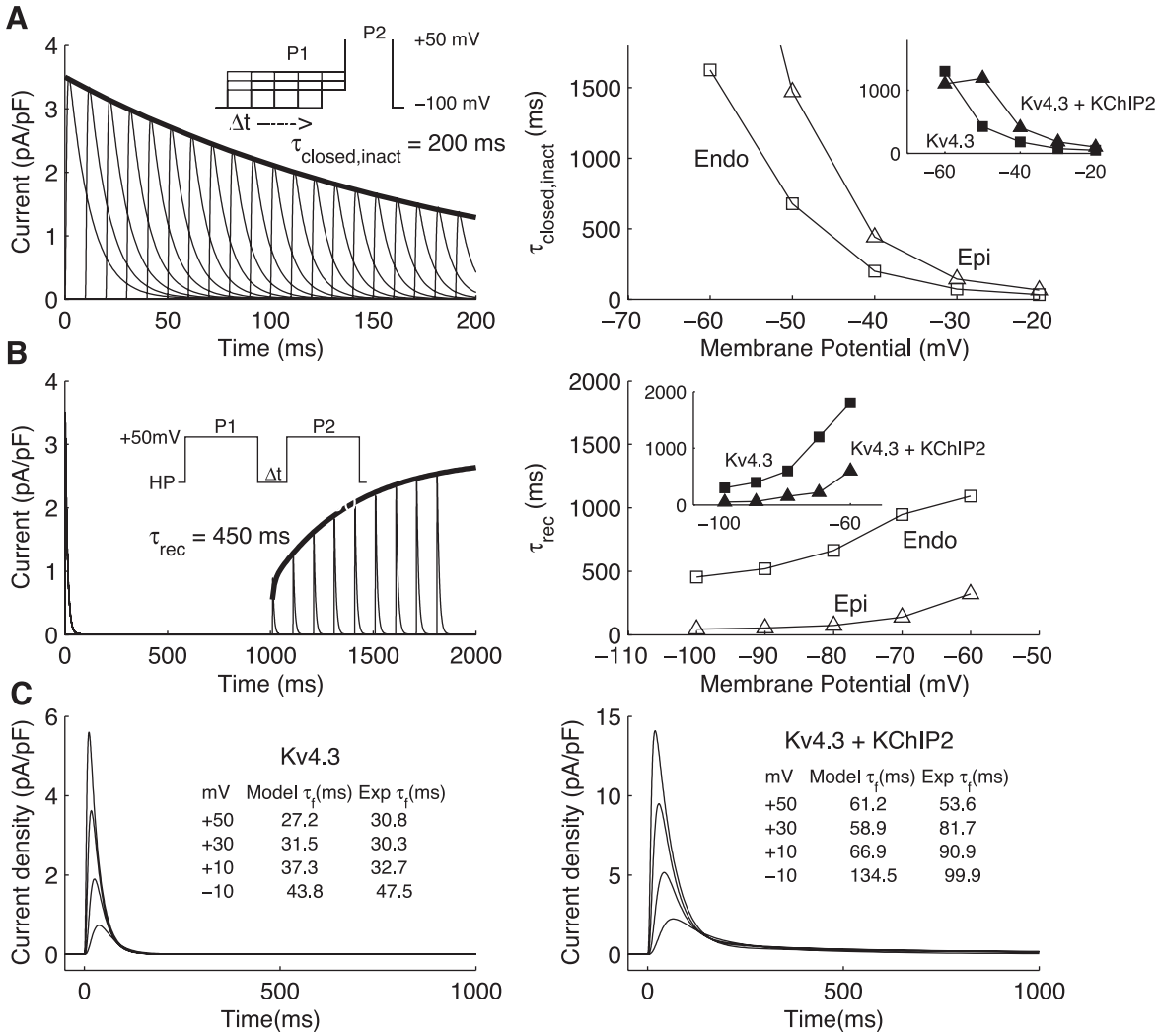

Fig. 2. Heterogeneity in the KChIP2-dependent gating kinetics of I_{Kv43} in epicardial and endocardial canine LV myocytes over a range of examined potentials. *A*: voltage dependence of Kv4.3 closed-state inactivation kinetics (−60 to −20 mV) with representative Kv4.3 closed-state inactivation protocol current waveforms for P1 = −40 mV (*left*). Peak P2 currents were fitted with a single exponential relationship with indicated $\tau_{closed,inact}$. *Inset*: voltage-clamp protocol. *Right*: overlay of the predicted time constants of closed-state inactivation. *Inset*: experimental data of Patel et al. (42), with averaged results for different KChIP2 isoforms. *B*: voltage dependence of Kv4.3 recovery kinetics (−100 mV to −60 mV) with representative Kv4.3 recovery waveforms at a holding potential (HP) = −100 mV fitted with indicated τ_{rec} (*left*). *Inset*: recovery protocol. *Right*: overlay of predicted values of τ_{rec} for Kv4.3 and Kv4.3 + KChIP2 isoforms. *Inset*: experimental data of Patel et al. (42).

closed-stated inactivation kinetics (Fig. 2*A*) were measured using a P2 pulse to +50 mV preceded by a P1 pulse of progressively increasing duration applied at a number of selected membrane potentials (see *inset* to Fig. 2*A* for protocol). The time course of this family of peak currents was well approximated by a single exponential with associated time constant, $\tau_{closed,inact}$. Note that the model predictions closely match the experimentally measured voltage dependence of closed-state inactivation. The effect of KChIP2 on steady-state inactivation is also reproduced very well. The experimentally measured mean value of $\tau_{closed,inact}$ at −60 mV for Kv4.3 with KChIP2 diverges from the exponential function that depicts the voltage dependence of closed-state inactivation kinetics at more depolarized potentials. Although the model fails to account for this deviation, it is unlikely to play a significant role in simulations of AP waveform, which are the main focus of this investigation.

The voltage dependence of Kv4.3 recovery kinetics was evaluated over the range −100 to −60 mV (Fig. 2*B*). A conventional double-pulse protocol (Fig. 2*B*, *inset*) was used in which interpulse intervals were varied at four selected holding potentials. Faster recovery kinetics for epicardial compared with endocardial cells were obtained at all holding potentials. Both plots are in agreement with experimental results. Midmyocardial myocyte transition rates for α_i, β_i, $\alpha_{o,i}$, and $\beta_{o,i}$ (not shown) were interpolated based on reported KChIP2 expression levels. Once again, all model predictions are within the bounds of reported experimental variation.

Macroscopic inactivation kinetics were examined over the voltage range from minimal to nearly maximal current activation (−30 to +50 mV). To test the ability of our models to yield inactivation rates, we fitted the time course of activated current decay to a single exponential function with associated

time constant τ_f and compared this with the experimentally measured values of Patel et al. (42) (Fig. 2*C*).

We then explored the consequences of a proposed Ca^{2+}-dependent inactivation of I_{Kv43} on the canine LV AP waveforms. Our simulations predict that Ca^{2+}-independent inactivation of I_{Kv43} alone results in a pronounced unphysiological delay of the AP plateau (i.e., prolongation of phase 1 of the AP) in epicardial and midmyocardial myocyte models (Fig. 3). This is not consistent with experimental data. In contrast, simulations in which inactivation proceeded via both Ca^{2+}-dependent and -independent mechanisms resulted in more realistic AP waveforms. These results suggest that KChIPs may modify I_{Kv43} in both a Ca^{2+}-dependent and -independent fashion.

The slowly inactivating or late Na^+ current, I_{NaL}. Figure 4*A* consists of computed records of I_{NaL} activated in response to a series of depolarizing steps (duration 700 ms) from −140 mV (to relieve inactivation) to voltages ranging from −60 mV to 0 mV. The resulting current-voltage relationship (Fig. 4*B*) closely matches the experimental measurements of Valdivia et al. (59) over much of the examined range of membrane potentials.

The slowly activating delayed rectifier current, I_{Ks}. These models predict a heterogeneous distribution of I_{Ks} tail currents (Fig. 5*A*) resulting from repolarization to −20 mV following a 5-s depolarizing stimulus (*inset* for Fig. 5*A* shows magnified view of the tail currents). The predicted current-voltage relationship (Fig. 5*B*) appears to reproduce the corresponding experimental findings by Liu and Antzelevitch (29) (*inset* for Fig. 5*B*) accurately.

The Ca^{2+}-activated chloride current, $I_{Cl(Ca)}$. These models of epicardial and midmyocardial myocytes include a small contribution of $I_{Cl(Ca)}$ to total transient outward current (Fig. 6). Note that the net effect of this was appropriate AP morphology and duration for these two myocyte subtypes. However, the lack of any significant outward current generated an abnormal phase 2 "hump" that delayed repolarization and prolonged APD_{90} in endocardial cells. Selectively increasing $I_{Cl(Ca)}$ in endocardial cells prevented this and resulted in an APD_{90} typical of these myocytes at this pacing rate (see DISCUSSION).

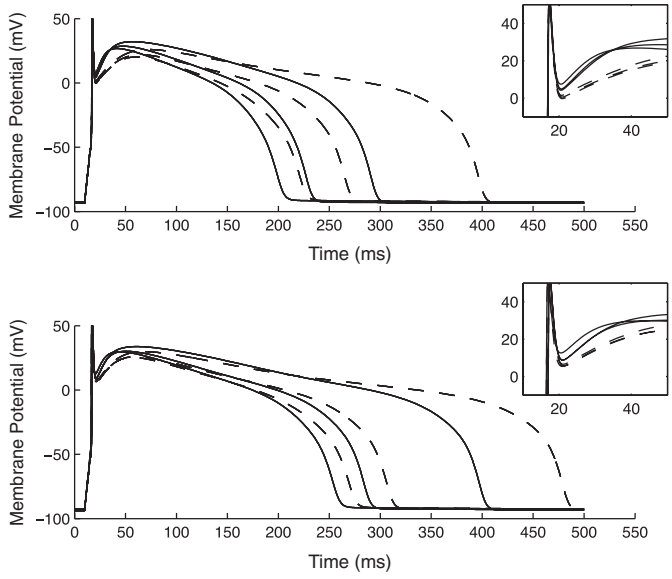

Fig. 3. Consequences of Ca^{2+}-independent only (dashed) vs. both $[Ca^{2+}]_i$-dependent and $[Ca^{2+}]_i$-independent (solid) mechanisms of I_{Kv43} inactivation in epicardial (*top*) and midmyocardial (*bottom*) myocyte models.

Ca^{2+} homeostasis and AP morphology in normal canine ventricular myocytes. A major requirement of mathematical models of cardiac myocyte electrophysiology and ECC is the ability to accurately simulate qualitative and quantitative changes in the AP and Ca^{2+} transient, as a function of pacing frequency and LV location. In Fig. 7, we demonstrate the ability of our model to predict Ca^{2+} cycling kinetics that are consistent with the experimental results of Cordeiro et al. (8). Specifically, an enhanced greater SR Ca^{2+} content and faster Ca^{2+} transient decay rates are observed in myocytes from the LV epicardium.

Figure 8 shows the resulting APs at cycle lengths of 500, 1,000, and 2,000 ms in the three canine ventricular myocytes subtypes. Table 1 compares the predicted APD_{90} with the experimentally measured values of Liu and Antzelevitch (29). In all cases the model predictions are within one standard deviation of the experimentally reported means.

We also explored the extent to which early repolarization currents play a role in determining the differences in APD between epicardial, midmyocardial, and endocardial myocytes at varying pacing rates. APD_{30} was measured and compared with APD_{90}. In all cases, the most significant difference was observed at APD_{30}. The difference times (APD_{90} − APD_{30}) showed very little dependence on pacing rate and myocyte subtype.

Our models can be used to investigate the relative contribution of each known heterogeneity to prolongation of the midmyocardial AP (Table 2). We systematically switched midmyocardial parameters relating to each heterogeneous current to epicardial parameters. Specifically, the perturbations were as follows: G_{NaL} = 1.15 mS/uF, G_{Ks} = 0.02 mS/uF, k_{SR} = 2.0, and all epicardial I_{Kv43} parameters. Using the model, we found that modifying I_{NaL} and I_{Kv43} parameters resulted in the most significant rate-dependent impact on APD_{30}. Substituting midmyocardial for epicardial I_{Kv43} parameters *1*) decreased I_{Kv43} conductance and *2*) altered the KChIP-dependent effects on I_{Kv43} inactivation. The KChIP modulation of I_{Kv43} played the major role in shortening APD_{30} (a mere decrease in I_{Kv43} conductance without modulation of KChIP-dependent kinetic parameters made little difference to APD measurements). I_{Ks} did not appear to contribute significantly to midmyocardial rate-dependent APD prolongation under physiological conditions. No perturbations resulted in large changes to the difference between APD_{90} and APD_{30}, suggesting that early repolarization currents dominate transmural heterogeneities in AP morphology.

Proarrhythmia due to the SCN5A-I1768V mutation. An enhancement of I_{NaL}, as in the case of the I1768V mutation (47), did not appear to alter early repolarization in any of the three myocyte subtypes. However, we observed EADs in both midmyocardial and endocardial myocytes that occurred at all examined stimulation cycle lengths (Fig. 9). This pattern of results may suggest that the sustained component of I_{Kv43} cannot only produce rapid early repolarization in epicardial myocytes but may also protect against the late increase in I_{Na} and subsequent EAD formation.

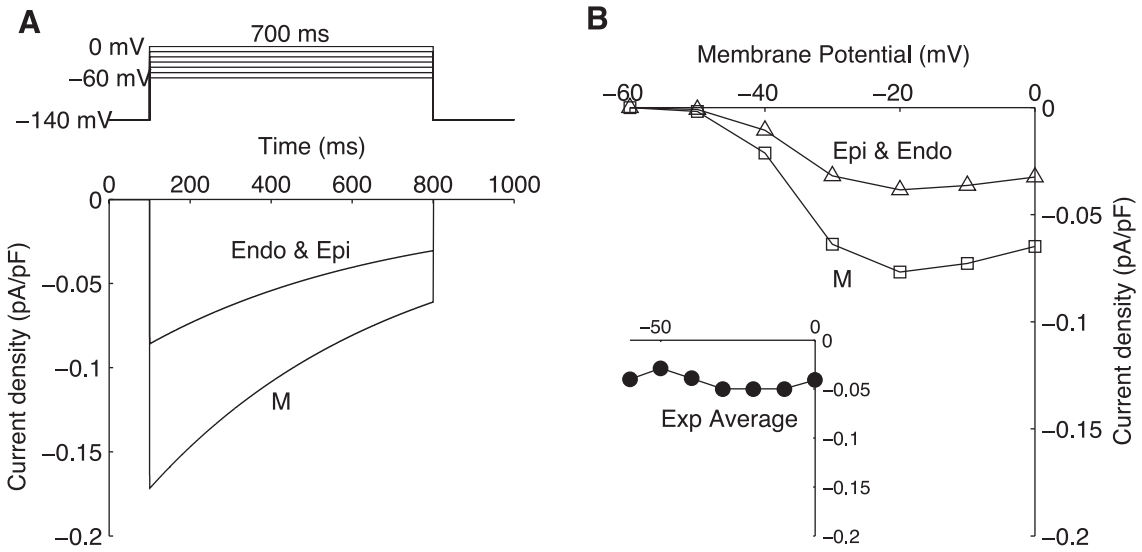

Fig. 4. Heterogeneity of I_{NaL}. *A*: voltage-clamp protocol and resulting currents at −20 mV at 25°C. *B*: model predictions of current-voltage relationship at 25°C (*inset*: Ref. 59, experimental results of Valdivia et al., room temperature).

DISCUSSION

Current and voltage-clamp studies of isolated canine ventricular myocytes have provided a wealth of quantitative data concerning the electrophysiological properties of the Na^+, Ca^{2+}, and K^+ and Cl^- currents that underlie the AP and contribute to AP heterogeneity. Information regarding the way in which individual subunits of ion channels can contribute to the electrical functioning of the ion channels has also been obtained. Evidence is emerging that in many instances, ion channels are components of macromolecular complexes, containing both pore-forming (α) and accessory (β or δ) subunits, and their function may be modified by a variety of regulatory proteins (38).

The transient outward K^+ current, I_{Kv43}. It has been suggested by many investigators that KChIPs can regulate the transmural heterogeneity of I_{Kv43} in canine ventricular myocytes (41). In addition to altering expression levels and accelerating recovery from inactivation, KChIP2 isoforms can modify Kv4.3 gating kinetics by *1*) a Ca^{2+}-independent slowing of closed-state inactivation and *2*) a $[Ca^{2+}]_i$-dependent open-state inactivation. This current was previously thought to be insensitive to $[Ca^{2+}]_i$, and previous models do not account for this.

The experimental data and proposed model of Patel et al. (42) predict that channels that inactivate by the open-state mechanism must reopen upon hyperpolarization before reentering the closed state (see Fig. S1 in the Supplemental Data). Such reopening events can generate an outward current. This current has been measured experimentally (9, 42, 50) and is maximal under conditions of elevated $[Ca^{2+}]_i$. In the model we

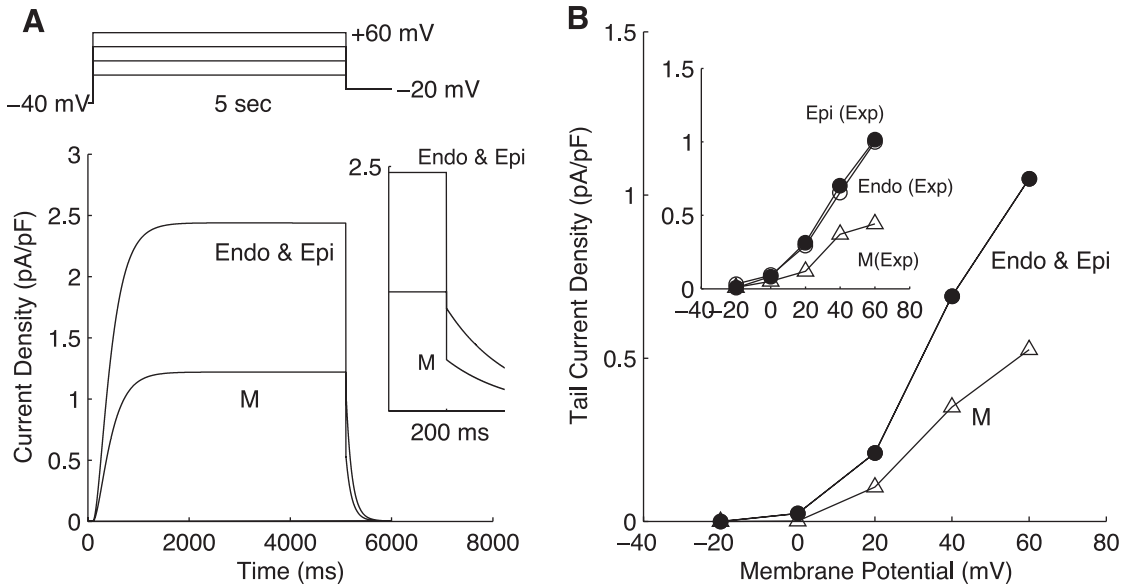

Fig. 5. Heterogeneity of I_{Ks} tail currents. *A*: model tracings of I_{Ks} depolarization and tail currents and voltage-clamp protocol at 37°C. *B*: voltage dependence of model (37°C) vs. experimental tail currents (*inset*: Ref. 29, Liu and Antzelevitch, 35–37°C).

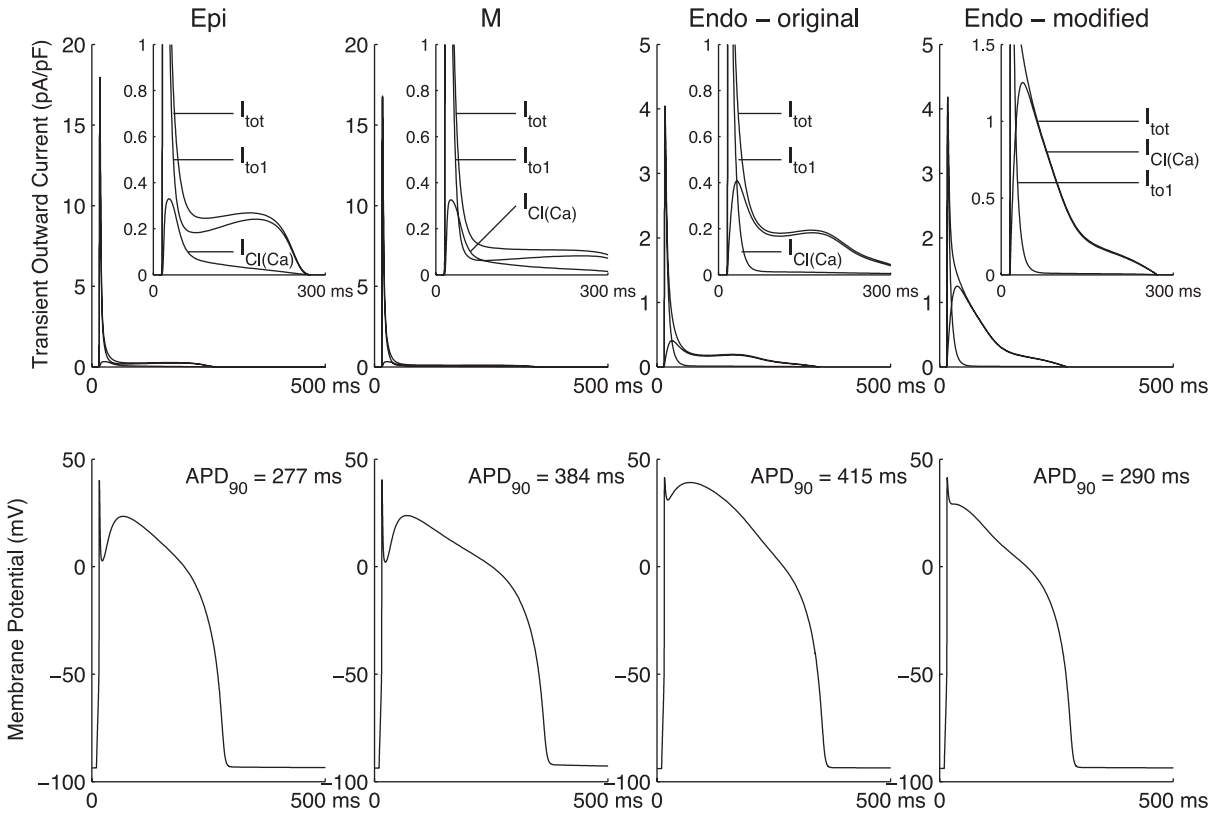

Fig. 6. Contributions of I_{Kv43} and $I_{Cl(Ca)}$ to total (I_{tot}) transient outward currents (*top*) in the three myocyte subtypes at a cycle length of 2,000 ms with corresponding action potentials (*bottom*). A modified endocardial cell model is included to demonstrate how an increase in $I_{Cl(Ca)}$ increases endocardial transient outward current preventing unphysiological features of action potential morphology and duration.

have developed, I_{Kv43} is most prominent in phase 1 but can also contribute to early repolarization since it fails to inactivate completely and can neutralize the sustained component of I_{Na}. This slow inactivation occurs as a consequence of KChIP2- and $[Ca^{2+}]_i$-dependent modifications to I_{Kv43} gating kinetics. This effect may become important in conditions such as congestive heart failure, when I_{Kv43} is significantly downregulated and APD_{90} is prolonged.

The hydrophobic interactions of KChIPs and Kv4 channels bear a striking resemblance to the modes of interaction between calmodulin and its target proteins (65). KChIPs and calmodulin moieties share the structural feature of a 4 EF-hand

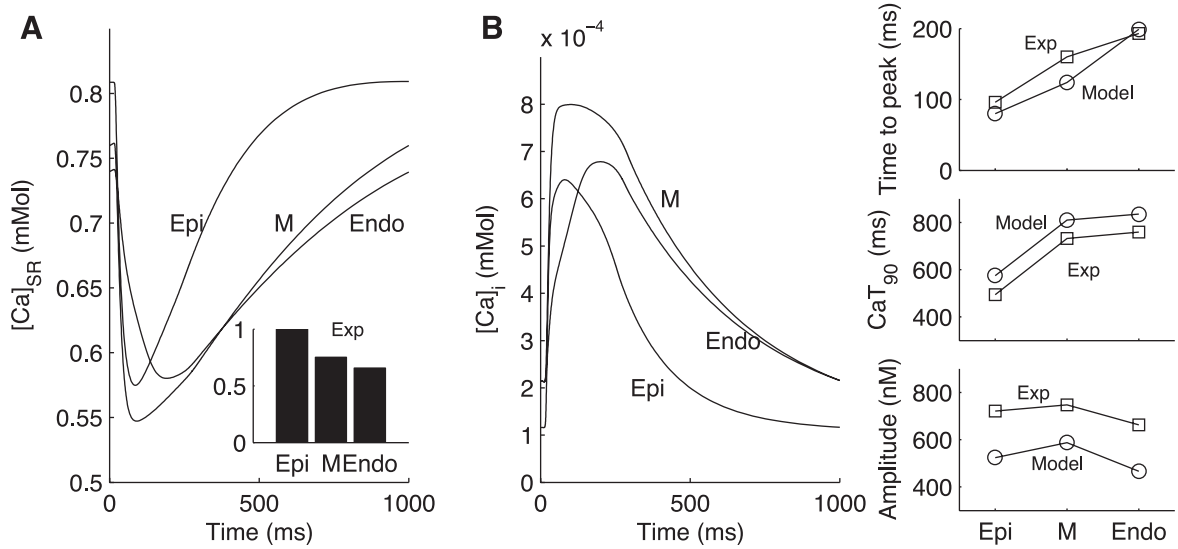

Fig. 7. Heterogeneity of sarcoplasmic reticulum (SR) Ca^{2+} concentration ($[Ca]_{SR}$, *A*) and Ca^{2+} transients ($[Ca]_i$, *B*) at 1 Hz with plotted comparisons between model predictions and measured experimental data of Cordeiro et al. (8). *Inset* in *A*: Cordeiro et al. (8).

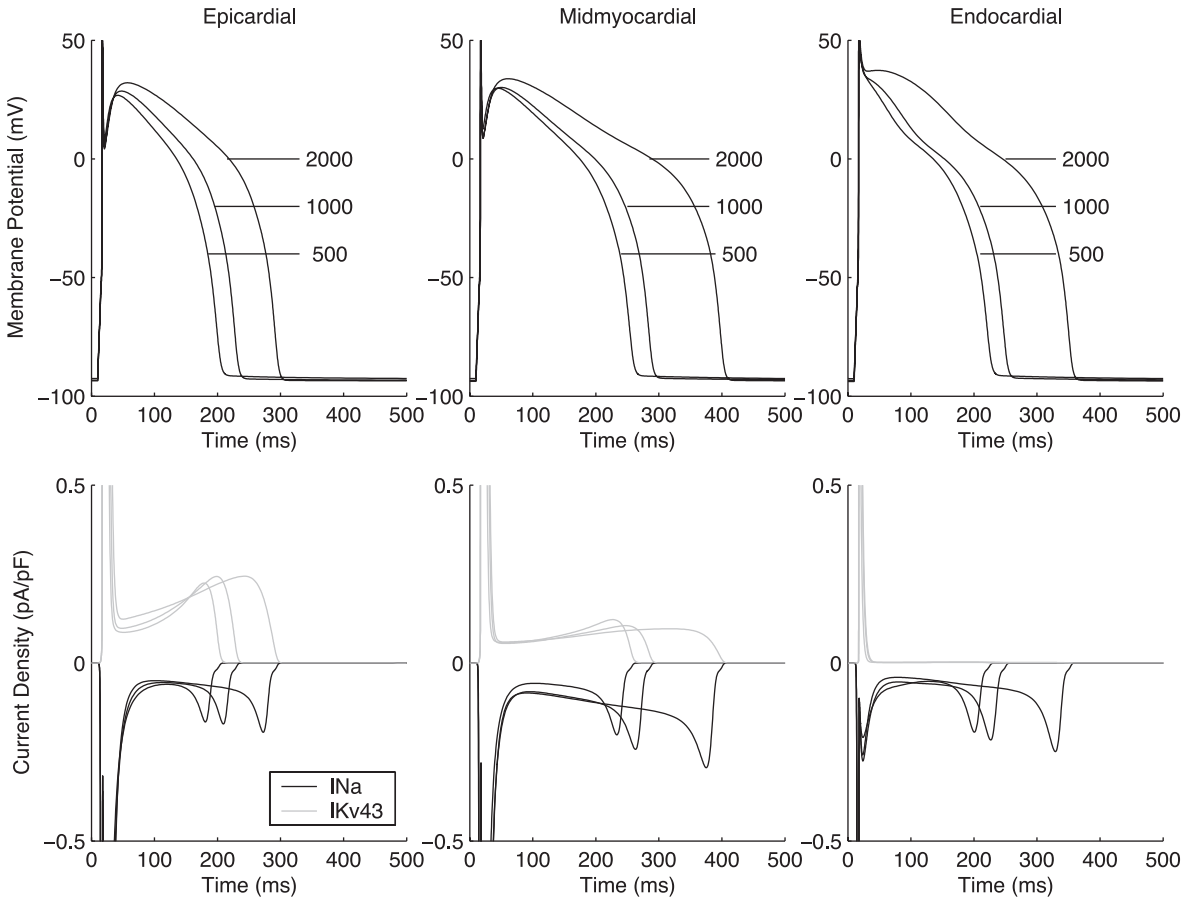

Fig. 8. *Top*: model-computed action potential morphology, duration, and rate dependence of epicardial, midmyocardial, and endocardial action potentials with parameters as outlined in the Supplemental Data. *Bottom*: model-computed I_{Na} (black) and I_{Kv43} (gray). Cycle lengths are in milliseconds.

scaffold that undergoes Ca^{2+}-mediated conformational changes. Furthermore, elution profiles from size-exclusion chromatography have indicated that chelating Ca^{2+} destabilizes the KChIP2-Kv4 interactions (65), consistent with similar results on calmodulin ion channel interaction. These and other studies suggest a common mechanism of Ca^{2+} regulation among ion channel proteins.

The slowly inactivating or late Na^+ current, I_{NaL}. In heart, the SCN5A-encoded Nav1.5 is the predominant carrier of I_{Na}. Accessory subunits also modulate I_{Na} current density and voltage-dependent gating (38). Recent evidence suggests that Na^+ channels contribute not only to the AP upstroke but also to the plateau phase and repolarization. Sustained activity can result from channels that fail to inactivate or channels that recover from inactivation during repolarization. A recent report by Maltsev and Undrovinas (32) delineates the behavior into three separate mechanisms: channel bursting, window current, and recovery from inactivation. Here we demonstrate that the sustained component of I_{Na} can be a potent regulator of early repolarization and underlies to a large extent the increase in the measured APDs and rate dependency of midmyocardial myocytes.

The I1768V mutation-induced increase in I_{NaL} is a potent instigator of Ca^{2+}-mediated EADs originating during phase 3

Table 1. *APD values in model compared with measurements of Liu and Antzelevitch (Ref. 29)*

		Experiment (Ref. 29)		Model		
	BCL, ms	APD_{90}, ms (Mean)	APD_{90}, ms (SD)	APD_{90}, ms	APD_{30}, ms	$APD_{90} - APD_{30}$, ms
Epicardial	500	197	35	186	131	55
	1,000	231	44	214	159	55
	2,000	250	47	277	219	58
Midmyocardial	500	222	29	241	177	64
	1,000	286	49	270	202	68
	2,000	338	77	384	303	81
Endocardial	500	212	28	209	139	70
	1,000	250	33	233	162	71
	2,000	270	40	290	216	74

APD, action potential duration; BCL, basic cycle length.

Table 2. *Prolongation of midmyocardial action potential*

	BCL, ms	APD_{90}, ms	APD_{30}, ms	$APD_{90} - APD_{30}$, ms	%Change From Baseline
Normal	500	241	177	64	
	1,000	270	202	68	
	2,000	384	303	81	
Epi G_{NaL}	500	233	169	64	3.32%
	1,000	254	190	64	5.93%
	2,000	345	274	71	10.16%
Epi G_{Ks}	500	238	174	64	1.24%
	1,000	266	198	68	1.48%
	2,000	365	287	78	4.95%
Epi k_{SR}	500	230	165	65	4.56%
	1,000	251	157	94	7.04%
	2,000	371	296	75	3.39%
Epi I_{Kv43}	500	225	167	58	6.64%
	1,000	246	185	61	8.89%
	2,000	329	264	65	14.32%

Epi, epicardial.

repolarization in our model. Specifically, this mutant has been demonstrated to result in long QT-syndrome type-3 (LQT3). Previous modeling studies of this mutation have suggested that the alteration in gating kinetics accounts for AP prolongation and susceptibility to Ca^{2+}-mediated EADs (7). Our simulations demonstrate that these phenotypes are most pronounced in midmyocardial and endocardial myocytes. These effects are also more marked in our canine models than previous modeling studies (in guinea pig) have suggested.

The slowly activating delayed rectifier current, I_{Ks}. Some previous models of the ionic currents that underlie the mammalian ventricular APs have tended to overestimate the magnitude of I_{Ks}. This may have been a practical adjustment made in order to exceed inward currents and hence generate the

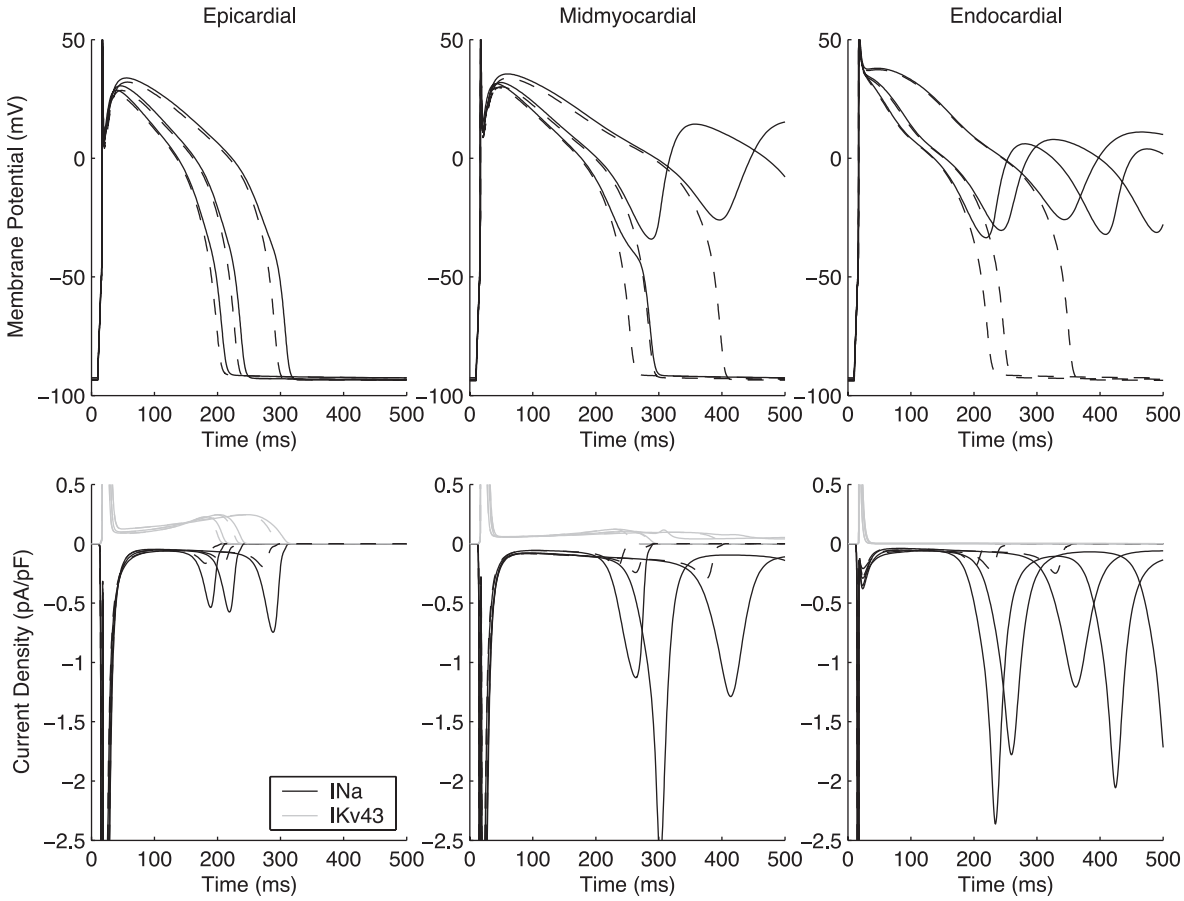

Fig. 9. *Top*: model-computed action potential morphology, duration, and rate dependence of epicardial, midmyocardial, and endocardial action potentials with altered I_{Na} parameters representative of the SCN5A-I1768V mutation. Original action potential tracings are shown in dashed lines for direct comparison. *Bottom*: model-computed I_{Na} (black) and I_{Kv43} (gray) for mutation with original currents shown in dashed lines for comparison. Cycle lengths are in milliseconds.

appropriate APD_{90}. It may also have contributed to the role of I_{Ks} in AP heterogeneity being overstated. Increasing the conductance of I_{Ks} in the midmyocardium to be equal to that in the other two regions decreased APD_{90} only slightly. Our results suggest that, under normal physiological conditions, other currents such as I_{NaL} and I_{Kv43} may have a greater influence on transmural heterogeneities of APD.

The Ca^{2+}-activated chloride current, $I_{Cl(Ca)}$. The extent to which anionic currents contribute to transmural electrical heterogeneity has been investigated less thoroughly than their cationic counterparts (20). No difference in $I_{Cl(Ca)}$ current density was measured in canine epicardial and midmyocardial myocytes (67), but endocardial myocytes were not included in this study. We could find no subsequent or prior report in the literature of an investigation into transmural heterogeneity of $I_{Cl(Ca)}$ in canines that included endocardial cells. Hence our decision to assign a heterogeneous transmural conductance of this current is not based on quantitative experimental results. Its inclusion in the model can be justified by the both the absence of conflicting data and clear evidence that without it, endocardial cells display unphysiological features of AP morphology.

Heterogeneities in Ca^{2+} fluxes and homeostasis. In canine LV myocytes, time to peak and the duration of the Ca^{2+} transient have been reported to be longer in endocardial cells (8). In addition, SR Ca^{2+} content, as measured by rapid application of caffeine, is largest in epicardial cells (8). A variety of experimental findings suggests that a combination of electrical heterogeneity and intrinsic differences in ECC may underlie these differences in the SR Ca^{2+} concentration and kinetics of the Ca^{2+} transients. Greater SERCA expression on the epicardium may contribute to a higher SR Ca^{2+} content and faster decay (25), while the spike and dome morphology of the epicardial AP waveform permits a greater LCC current (I_{CaL}) (15). It is presumed that these differences result in a more coordinated contraction of the ventricular myocardium, i.e., the faster kinetics of epicardial myocyte Ca^{2+} transients compensate for the delay in activation.

It is known that intracellular Ca^{2+} handling can have significant effects on cellular electrical behavior. Hence, it is very important to include mechanistic detail of intracellular Ca^{2+} dynamics in studies of the AP waveform. Many previous ionic models of ventricular myocyte ECC have dealt with intracellular Ca^{2+} cycling in only a qualitative manner. These approaches therefore lack a mechanistic representation of local Ca^{2+}-induced Ca^{2+} release control. For instance, common pool models, as their name suggests, direct Ca^{2+} influx and SR release into a single cytosolic domain, which simultaneously controls RyR current (22, 39, 40, 60). A consequence of this is that once the RyR current is triggered, the resulting increase in "subspace" Ca^{2+} ensures an all-or-none SR release. As such, these models fail to reproduce one of the most important features of Ca^{2+} handling in cardiac myocytes, that of the graded Ca^{2+} release, in which SR Ca^{2+} release is proportional to LCC influx (57). A further limitation of many previous models is their very strong reliance on voltage-dependent inactivation of I_{CaL} for stability (57). This conflicts with experimental evidence that consistently points to Ca^{2+}-dependent inactivation as the dominant mechanism (28). Other model formulations that base SR Ca^{2+} release on LCC influx do so in a phenomenological manner and have less predictive capability (13, 31, 44). In contrast, local control models (16, 46, 53, 55) have successfully reproduced experimental observations. However, in general, these are too computationally intensive for upward integration into tissue or whole organ models. Our model effectively addresses these limitations.

Limitations. Our model, in its present form, has several limitations. The existence of apparent discrepancies between the measured I_{NaCa} data of Zygmunt et al. (69), that of Xiong et al. (62), and the existing model formulation of I_{NaCa} prevented the inclusion of transmural heterogeneity of this current in this study. The disparities may have arisen from differences in experimental protocols and/or the difficulties associated with isolating this current using the required pharmacological approaches. To reconcile the differences in predicted I_{NaCa} heterogeneities, further experimental investigation is required. Thereafter, a thorough analysis of this antiporter mechanism can be carried out.

Our model recapitulates many of the observed differences between Kv4.3 currents expressed alone and with KChiPs in heterologous systems. However, it fails to predict $\tau_{closed,inact}$ at membrane potentials more negative than -50 mV. Furthermore, despite the evidence favoring two distinct mechanisms of inactivation, the current records were in most cases well-characterized with a single exponential with kinetics corresponding to the fast component (τ_f) of the results of Patel et al. (42). There may be several reasons for these discrepancies. First, it is difficult to predict intracellular Ca^{2+} concentrations (which are thought to regulate the slow component of inactivation) within the heterologous system. Second, as in the case of I_{Na}, multiple open states may underlie the different components of inactivation rate. Finally, many other mechanisms of Kv4 channel regulation have been demonstrated (see below).

Kuo et al. (24) have demonstrated the importance of KChIPs in the regulation of Kv4 channels by analyzing currents in right ventricular myocytes isolated from $KChIP^{-/-}$ mice. Their studies reveal a complete loss of I_{to1} in the RV of $KChIP^{-/-}$ mice. The majority of experimental reports confirms the importance of KChIPs in the regulation of I_{Kv43}. However, Deschenes et al. (10) failed to detect a transmural gradient of KChIP across the canine LV wall. It has been suggested that nonspecific binding of the polyclonal antibody used in this study may have masked the KChIP expression profile (41).

Many other mechanisms of Kv4 channel regulation have been demonstrated, and we do not account for these in our model (for a review see Patel and Campbell, Ref. 41). Briefly, these other regulatory subunits include frequenin (37), MinK-related peptide 1 (MiRP1) (64), NFAT/calcineurin (49), and DPPXs (36). All of these may contribute to I_{Kv43} regulation in vivo. Of these, frequenin is thought to be the most likely candidate (41), possibly due to the structural similarity to KChIPs (both are neuronal Ca^{2+} sensors containing multiple EF hands). Indeed, frequenin has been reported to coimmunoprecipitate with Kv4.3 α-subunits in mouse ventricle extracts (18). However, others were unable to detect this association (45). Furthermore, it has been demonstrated that the interactions of KChIPs with Kv4 channels are substantially stronger and/or more efficient than those of frequenin (45).

We have replicated and normalized model simulations as closely as possible to experimental data acquisition conditions and protocols. However, in some articles, a narrow temperature range was given instead of an exact value. The reaction rate

measurement Q_{10} is ~3 for gating kinetics and ~1.3 for ion transfer, which may introduce small errors into our predictions. Nevertheless, these errors are well within the bounds of normal experimental variation. Furthermore, the results from extrapolating kinetic data to 37°C are in close agreement with independent data.

Some of the results used in the validation process were obtained in heterologous cell culture systems. Additional modulating proteins, such as caveolins (63), present in the native environment of the cardiac myocyte sarcolemma, may affect channel function. We also failed to account for any interactions between ion channels and the actin cytoskeleton and/or the extracellular matrix, which have been suggested to play a role in whole-cell functioning (38).

Recent results also draw attention to a transmural gradient of the α-subunit of the Na^+-K^+ pump, I_{NaK}, in which ion channel expression decreases from epicardium to endocardium (14). However, it is thought that under physiological conditions, transmural gradients of intracellular Na^+ result in nearly homogeneous whole-cell I_{NaK}. The paucity of quantitative data regarding these results prohibited the inclusion of this electrochemical gradient in our investigation. There also appears to be a gradient of $I_{Cl(cAMP)}$, increasing from endocardium to epicardium (23, 58, 61). However, under normal conditions, cAMP levels are low and constant, and thus this current is unlikely to significantly contribute to cellular electrical response.

The Greenstein model (15) is based on dynamic changes in intracellular ion concentrations and as such displays some degree of time-dependent "drift." However, it is stable (in terms of both APD and intracellular ion concentrations to within 1.5%) over a period of greater than 50 heartbeats. This degree of stability is comparable, or better, than previous models of this type (34, 60).

Dixon et al. (11) report that Kv1.4 mRNA is present at 16% of the level of Kv4.3 mRNA in the canine LV. However, there appears to be no electrophysiological evidence for a Kv1.4-mediated slowly recovering cumulatively inactivating transient outward current phenotype in canine (41). With respect to the original Greenstein model (15), we have attempted to make only those changes that confer the molecular bases of transmural electrophysiological heterogeneities. Therefore, we have modified the original model of Greenstein et al. (15) to reflect the data of Dixon et al. (11) by decreasing the contribution of the Kv1.4 current but chose not to remove it completely. There is very strong evidence that Kv1.4 encodes the slow component of the transient outward current (41). Transmural heterogeneity of this current has been measured in the ferret and human LV (5, 35). We did not account for this heterogeneity in our model.

Recent experimental investigations suggest that calmodulin binding to KCNQ1, the pore-forming subunit of the I_{Ks} channel, is required for protein assembly and conferral of Ca^{2+} sensitivity to the I_{Ks} current (52). The role of calmodulin in the folding and assembly of KCNQ1 is likely to be accounted for indirectly in existing formulations of I_{Ks}. However, we do not model a Ca^{2+} sensitive component of I_{Ks}. Although we do not account for this potentially important mechanism of functional regulation of I_{Ks}, we demonstrate only a minimal contribution of I_{Ks} to repolarization in canine ventricular myocytes under our simulation conditions. Further investigations into AP regulation during elevated adrenergic tone may require these interactions to be incorporated into the model.

Suggested experiments. One of the consequences of detailed model development and testing is that it reveals where the published experimental results in single myocytes fail to fully account for physiological phenomena. Our results suggest a number of potential opportunities for further investigation, including additional examination of transient outward currents in canine endocardial myocytes and the detailed nature of the transmural heterogeneity of I_{NaCa}.

Our model may also be a useful tool to aid in the understanding of arrhythmia mechanisms in patients with Brugada syndrome. This condition is characterized by ST segment elevation, prominent J-waves, and sudden cardiac death (1). Brugada syndrome appears to be linked to SCN5A mutations that result in a reduction of Na^+ influx across the right ventricular epicardium (26). It is hypothesized that premature repolarization in this region contributes to electrical heterogeneity of repolarization and creates an electrical substrate conducive to reentrant arrhythmias (1).

Summary. We have completed meaningful modifications to the Greenstein model (15) of canine midmyocardial myocyte ECC for epicardial and endocardial cells. Expression levels (current densities) and gating kinetics parameters for I_{Kv43}, I_{Ks}, I_{NaL}, and SERCA were constrained by experimental data from a number of different laboratories, using myocytes isolated from the three transmural locations within the canine LV. Our results suggest that early repolarization currents such as I_{Kv43} and I_{NaL} play a major role in shaping the cardiac AP. The model predicted that KChIP2- and Ca^{2+}-dependent control of I_{Kv43} permits a sustained outward current that neutralizes I_{NaL} in a rate- and subtype-dependent manner. Both these currents appear to play major roles in the increased AP duration and rate dependence in midmyocardial myocytes. Furthermore, the increased ratio of I_{Kv43} to I_{NaL} appears to protect epicardial myocytes, since the incidence of EADs resulting from the SCN5A-I1768V mutation-induced increase in I_{NaL} is much reduced.

ACKNOWLEDGMENTS

We gratefully acknowledge the generosity of Drs. Joseph Greenstein and Colleen Clancy in providing code for the original midmyocardial myocyte model and I_{Na} Markov model, respectively.

GRANTS

This work was supported by an American Heart Association Predoctoral Fellowship (to S. N. Flaim), National Biomedical Computation Resource Grant P41RR-08605 (to A. D. McCulloch), and National Science Foundation Grant BES-0506252 (to A. D. McCulloch).

REFERENCES

1. **Antzelevitch C.** Ion channels and ventricular arrhythmias: cellular and ionic mechanisms underlying the Brugada syndrome. *Curr Opin Cardiol* 14: 274–279, 1999.
2. **Antzelevitch C and Fish J.** Electrical heterogeneity within the ventricular wall. *Basic Res Cardiol* 96: 517–527, 2001.
3. **Anyukhovsky EP, Sosunov EA, and Rosen MR.** Regional differences in electrophysiological properties of epicardium, midmyocardium, and endocardium: in vitro and in vivo correlations. *Circulation* 94: 1981–1988, 1996.
4. **Bers DM.** Cardiac excitation-contraction coupling. *Nature* 415: 198–205, 2002.
5. **Brahmajothi MV, Campbell DL, Rasmusson RL, Morales MJ, Trimmer JS, Nerbonne JM, and Strauss HC.** Distinct transient outward

potassium current (Ito) phenotypes and distribution of fast-inactivating potassium channel alpha subunits in ferret left ventricular myocytes. *J Gen Physiol* 113: 581–600, 1999.

6. **Brunet S, Aimond F, Li H, Guo W, Eldstrom J, Fedida D, Yamada KA, and Nerbonne JM.** Heterogeneous expression of repolarizing, voltage-gated K^+ currents in adult mouse ventricles. *J Physiol* 559: 103–120, 2004.
7. **Clancy CE, Tateyama M, Liu H, Wehrens XH, and Kass RS.** Non-equilibrium gating in cardiac Na^+ channels: an original mechanism of arrhythmia. *Circulation* 107: 2233–2237, 2003.
8. **Cordeiro JM, Greene L, Heilmann C, Antzelevitch D, and Antzelevitch C.** Transmural heterogeneity of calcium activity and mechanical function in the canine left ventricle. *Am J Physiol Heart Circ Physiol* 286: H1471–H1479, 2004.
9. **Demo SD and Yellen G.** The inactivation gate of the Shaker K^+ channel behaves like an open-channel blocker. *Neuron* 7: 743–753, 1991.
10. **Deschenes I, DiSilvestre D, Juang GJ, Wu RC, An WF, and Tomaselli GF.** Regulation of Kv4.3 current by KChIP2 splice variants: a component of native cardiac I(to)? *Circulation* 106: 423–429, 2002.
11. **Dixon JE, Shi W, Wang HS, McDonald C, Yu H, Wymore RS, Cohen IS, and McKinnon D.** Role of the Kv4.3 K^+ channel in ventricular muscle. A molecular correlate for the transient outward current. *Circ Res* 79: 659–668, 1996.
12. **Drouin E, Charpentier F, Gauthier C, Laurent K, and Le Marec H.** Electrophysiologic characteristics of cells spanning the left ventricular wall of human heart: evidence for presence of M cells. *J Am Coll Cardiol* 26: 185–192, 1995.
13. **Faber GM and Rudy Y.** Action potential and contractility changes in $[Na^+]_i$ overloaded cardiac myocytes: a simulation study. *Biophys J* 78: 2392–2404, 2000.
14. **Gao J, Wang W, Cohen IS, and Mathias RT.** Transmural gradients in Na/K pump activity and $[Na^+]_i$ in canine ventricle. *Biophys J* 89: 1700–1709, 2005.
15. **Greenstein JL, Hinch R, and Winslow RL.** Mechanisms of excitation-contraction coupling in an integrative model of the cardiac ventricular myocyte. *Biophys J* 90: 77–91, 2006.
16. **Greenstein JL and Winslow RL.** An integrative model of the cardiac ventricular myocyte incorporating local control of Ca^{2+} release. *Biophys J* 83: 2918–2945, 2002.
17. **Greenstein JL, Wu R, Po S, Tomaselli GF, and Winslow RL.** Role of the calcium-independent transient outward current I(to1) in shaping action potential morphology and duration. *Circ Res* 87: 1026–1033, 2000.
18. **Guo W, Malin SA, Johns DC, Jeromin A, and Nerbonne JM.** Modulation of Kv4-encoded K^+ currents in the mammalian myocardium by neuronal calcium sensor-1. *J Biol Chem* 277: 26436–26443, 2002.
19. **Hinch R, Greenstein JL, Tanskanen AJ, Xu L, and Winslow RL.** A simplified local control model of calcium-induced calcium release in cardiac ventricular myocytes. *Biophys J* 87: 3723–3736, 2004.
20. **Hume JR, Duan D, Collier ML, Yamazaki J, and Horowitz B.** Anion transport in heart. *Physiol Rev* 80: 31–81, 2000.
21. **Iyer V, Mazhari R, and Winslow RL.** A computational model of the human left-ventricular epicardial myocyte. *Biophys J* 87: 1507–1525, 2004.
22. **Jafri MS, Rice JJ, and Winslow RL.** Cardiac Ca^{2+} dynamics: the roles of ryanodine receptor adaptation and sarcoplasmic reticulum load. *Biophys J* 74: 1149–1168, 1998.
23. **James AF, Tominaga T, Okada Y, and Tominaga M.** Distribution of cAMP-activated chloride current and CFTR mRNA in the guinea pig heart. *Circ Res* 79: 201–207, 1996.
24. **Kuo HC, Cheng CF, Clark RB, Lin JJ, Lin JL, Hoshijima M, Nguyen-Tran VT, Gu Y, Ikeda Y, Chu PH, Ross J, Giles WR, and Chien KR.** A defect in the Kv channel-interacting protein 2 (KChIP2) gene leads to a complete loss of I(to) and confers susceptibility to ventricular tachycardia. *Cell* 107: 801–813, 2001.
25. **Laurita KR, Katra R, Wible B, Wan X, and Koo MH.** Transmural heterogeneity of calcium handling in canine. *Circ Res* 92: 668–675, 2003.
26. **Leroy SS and Russell M.** Long QT syndrome and other repolarization-related dysrhythmias. *AACN Clin Issues* 15: 419–431, 2004.
27. **Li GR, Feng JL, Carrier M, and Nattel S.** Transmural electrophysiologic heterogeneity in the human ventricle. *Circulation* 92: 750–750, 1995.
28. **Linz KW and Meyer R.** Control of L-type calcium current during the action potential of guinea-pig ventricular myocytes. *J Physiol* 513: 425–442, 1998.
29. **Liu DW and Antzelevitch C.** Characteristics of the delayed rectifier current (IKr and IKs) in canine ventricular epicardial, midmyocardial, and endocardial myocytes: a weaker IKs contributes to the longer action potential of the M cell. *Circ Res* 76: 351–365, 1995.
30. **Liu DW, Gintant GA, and Antzelevitch C.** Ionic bases for electrophysiological distinctions among epicardial, midmyocardial, and endocardial myocytes from the free wall of the canine left ventricle. *Circ Res* 72: 671–687, 1993.
31. **Luo CH and Rudy Y.** A dynamic model of the cardiac ventricular action potential. I. Simulations of ionic currents and concentration changes. *Circ Res*: 1071–1096, 1994.
32. **Maltsev VA and Undrovinas AI.** A multi-modal composition of the late Na^+ current in human ventricular cardiomyocytes. *Cardiovasc Res* 69: 116–127, 2006.
33. **McIntosh MA, Cobbe SM, and Smith GL.** Heterogeneous changes in action potential and intracellular Ca^{2+} in left ventricular myocyte subtypes from rabbits with heart failure. *Cardiovasc Res* 45: 397–409, 2000.
34. **Michailova A and McCulloch A.** Model study of ATP and ADP buffering, transport of Ca^{2+} and Mg^{2+}, and regulation of ion pumps in ventricular myocyte. *Biophys J* 81: 614–629, 2001.
35. **Nabauer M, Beuckelmann DJ, Uberfuhr P, and Steinbeck G.** Regional differences in current density and rate-dependent properties of the transient outward current in subepicardial and subendocardial myocytes of human left ventricle. *Circulation* 93: 168–177, 1996.
36. **Nadal MS, Ozaita A, Amarillo Y, Vega-Saenz de Miera E, Ma Y, Mo W, Goldberg EM, Misumi Y, Ikehara Y, Neubert TA, and Rudy B.** The CD26-related dipeptidyl aminopeptidase-like protein DPPX is a critical component of neuronal A-type K^+ channels. *Neuron* 37: 449–461, 2003.
37. **Nakamura TY, Pountney DJ, Ozaita A, Nandi S, Ueda S, Rudy B, and Coetzee WA.** A role for frequenin, a Ca^{2+}-binding protein, as a regulator of Kv4 K^+-currents. *Proc Natl Acad Sci USA* 98: 12808–12813, 2001.
38. **Nerbonne JM and Kass RS.** Molecular physiology of cardiac repolarization. *Physiol Rev* 85: 1205–1253, 2005.
39. **Noble D, Varghese A, Kohl P, and Noble P.** Improved guinea-pig ventricular cell model incorporating a diadic space, IKr and IKs, and length- and tension-dependent processes. *Can J Cardiol* 14: 123–134, 1998.
40. **Pandit SV, Clark RB, Giles WR, and Demir SS.** A mathematical model of action potential heterogeneity in adult rat left ventricular myocytes. *Biophys J* 81: 3029–3051, 2001.
41. **Patel SP and Campbell DL.** Transient outward potassium current, "Ito", phenotypes in the mammalian left ventricle: underlying molecular, cellular and biophysical mechanisms. *J Physiol* 569: 7–39, 2005.
42. **Patel SP, Parai R, and Campbell DL.** Regulation of Kv4.3 voltage-dependent gating kinetics by KChIP2 isoforms. *J Physiol* 557: 19–41, 2004.
43. **Peterson BZ, DeMaria CD, Adelman JP, and Yue DT.** Calmodulin is the Ca^{2+} sensor for Ca^{2+}-dependent inactivation of L-type calcium channels. *Neuron* 22: 549–558, 1999.
44. **Priebe L and Beuckelmann DJ.** Simulation study of cellular electric properties in heart failure. *Circ Res* 82: 1206–1223, 1998.
45. **Ren X, Shand SH, and Takimoto K.** Effective association of Kv channel-interacting proteins with Kv4 channel is mediated with their unique core peptide. *J Biol Chem* 278: 43564–43570, 2003.
46. **Rice JJ, Jafri MS, and Winslow RL.** Modeling gain and gradedness of Ca^{2+} release in the functional unit of the cardiac diadic space. *Biophys J* 77: 1871–1884, 1999.
47. **Rivolta I, Clancy CE, Tateyama M, Liu H, Priori SG, and Kass RS.** A novel SCN5A mutation associated with long QT-3: altered inactivation kinetics and channel dysfunction. *Physiol Genomics* 10: 191–197, 2002.
48. **Rosati B, Pan Z, Lypen S, Wang HS, Cohen I, Dixon JE, and McKinnon D.** Regulation of KChIP2 potassium channel beta subunit gene expression underlies the gradient of transient outward current in canine and human ventricle. *J Physiol* 533: 119–125, 2001.
49. **Rossow CF, Dilly KW, and Santana LF.** Differential calcineurin/NFATc3 activity contributes to the Ito transmural gradient in the mouse heart. *Circ Res* 98: 1306–1313, 2006.
50. **Ruppersberg JP, Frank R, Pongs O, and Stocker M.** Cloned neuronal IK(A) channels reopen during recovery from inactivation. *Nature* 353: 657–660, 1991.
51. **Sah R, Ramirez RJ, Oudit GY, Gidrewicz D, Trivieri MG, Zobel C, and Backx PH.** Regulation of cardiac excitation-contraction coupling by

action potential repolarization: role of the transient outward potassium current (I(to)). *J Physiol* 546: 5–18, 2003.
52. **Shamgar L, Ma L, Schmitt N, Haitin Y, Peretz A, Wiener R, Hirsch J, Pongs O, and Attali B.** Calmodulin is essential for cardiac IKS channel gating and assembly: impaired function in long-QT mutations. *Circ Res* 98: 1055–1063, 2006.
53. **Shiferaw Y, Watanabe MA, Garfinkel A, Weiss JN, and Karma A.** Model of intracellular calcium cycling in ventricular myocytes. *Biophys J* 85: 3666–3686, 2003.
54. **Sicouri S and Antzelevitch C.** A subpopulation of cells with unique electrophysiological properties in the deep subepicardium of the canine ventricle. The M cell. *Circ Res* 68: 1729–1741, 1991.
55. **Soeller C and Cannell MB.** Numerical simulation of local calcium movements during L-type calcium channel gating in the cardiac diad. *Biophys J* 73: 97–111, 1997.
56. **Spitzer KW, Pollard AE, Yang L, Zaniboni M, Cordeiro JM, and Huelsing DJ.** Cell-to-cell electrical interactions during early and late repolarization. *J Cardiovasc Electrophysiol* 17, *Suppl* 1: S8–S14, 2006.
57. **Stern MD.** Theory of excitation-contraction coupling in cardiac muscle. *Biophys J* 63: 497–517, 1992.
58. **Takano M and Noma A.** Distribution of the isoprenaline-induced chloride current in rabbit heart. *Pflügers Arch* 420: 223–226, 1992.
59. **Valdivia CR, Chu WW, Pu J, Foell JD, Haworth RA, Wolff MR, Kamp TJ, and Makielski JC.** Increased late sodium current in myocytes from a canine heart failure model and from failing human heart. *J Mol Cell Cardiol* 38: 475–483, 2005.
60. **Winslow RL, Rice J, Jafri S, Marban E, and O'Rourke B.** Mechanisms of altered excitation-contraction coupling in canine tachycardia-induced heart failure. II. Model studies. *Circ Res* 84: 571–586, 1999.
61. **Wong KR, Trezise AE, Bryant S, Hart G, and Vandenberg JI.** Molecular and functional distributions of chloride conductances in rabbit ventricle. *Am J Physiol Heart Circ Physiol* 277: H1403–H1409, 1999.
62. **Xiong W, Tian Y, DiSilvestre D, and Tomaselli GF.** Transmural heterogeneity of Na^+-Ca^{2+} exchange: evidence for differential expression in normal and failing hearts. *Circ Res* 97: 207–209, 2005.
63. **Yarbrough TL, Lu T, Lee HC, and Shibata EF.** Localization of cardiac sodium channels in caveolin-rich membrane domains: regulation of sodium current amplitude. *Circ Res* 90: 443–449, 2002.
64. **Zhang M, Jiang M, and Tseng GN.** minK-related peptide 1 associates with Kv4.2 and modulates its gating function: potential role as beta subunit of cardiac transient outward channel? *Circ Res* 88: 1012–1019, 2001.
65. **Zhou W, Qian Y, Kunjilwar K, Pfaffinger PJ, and Choe S.** Structural insights into the functional interaction of KChIP1 with Shal-type K^+ channels. *Neuron* 41: 573–586, 2004.
66. **Zicha S, Xiao L, Stafford S, Cha TJ, Han W, Varro A, and Nattel S.** Transmural expression of transient outward potassium current subunits in normal and failing canine and human hearts. *J Physiol* 561: 735–748, 2004.
67. **Zygmunt AC.** Intracellular calcium activates a chloride current in canine ventricular myocytes. *Am J Physiol Heart Circ Physiol* 267: H1984–H1995, 1994.
68. **Zygmunt AC, Eddlestone GT, Thomas GP, Nesterenko VV, and Antzelevitch C.** Larger late sodium conductance in M cells contributes to electrical heterogeneity in canine ventricle. *Am J Physiol Heart Circ Physiol* 281: H689–H697, 2001.
69. **Zygmunt AC, Goodrow RJ, and Antzelevitch C.** I_{NaCa} contributes to electrical heterogeneity within the canine ventricle. *Am J Physiol Heart Circ Physiol* 278: H1671–H1678, 2000.